Nonequilibrium evolution of strong-field anisotropic ionized electrons towards a delayed plasma-state

B. Pasenow,[1,2,*] **J. V. Moloney,**[1,2] **S. W. Koch,**[2,3] **S. H. Chen,**[4] **A. Becker,**[4] **and A. Jaroń-Becker**[4]

[1]*Arizona Center for Mathematical Sciences, Department of Mathematics, University of Arizona, Tucson, Arizona 85721, USA*
[2]*College of Optical Sciences, University of Arizona, Tucson, Arizona 85721, USA*
[3]*Department of Physics and Material Sciences Center, Philipps-University, 35032 Marburg, Germany*
[4]*JILA and Department of Physics, University of Colorado at Boulder, Boulder, Colorado 80309-0440, USA*

[*]*pasenow@acms.arizona.edu*

Abstract: Rigorous quantum calculations of the femtosecond ionization of hydrogen atoms in air lead to highly anisotropic electron and ion angular (momentum) distributions. A quantum Monte-Carlo analysis of the subsequent many-body dynamics reveals two distinct relaxation steps, first to a nearly isotropic hot nonequilibrium and then to a quasi-equilibrium configuration. The collective isotropic plasma state is reached on a picosecond timescale well after the ultrashort ionizing pulse has passed.

References and links

1. T. Popmintchev, M.-C. Chen, P. Arpin, M. M. Murnane, and H. C. Kapteyn, "The attosecond nonlinear optics of bright coherent X-ray generation," Nat. Photonics **4**, 822–832 (2010).
2. A. Couairon and A. Mysyrowicz, "Femtosecond filamentation in transparent media," Phys. Rep. **441**, 47–189 (2007).
3. Y. Huismans, A. Rouzee, A. Gijsbertsen, J. H. Jungmann, A. S. Smolkowska, P. S. W. M. Logman, F. Lepine, C. Cauchy, S. Zamith, T. Marchenko, J. M. Bakker, G. Berden, B. Redlich, A. F. G. van der Meer, H. G. Muller, W. Vermin, K. J. Schafer, M. Spanner, M. Y. Ivanov, O. Smirnova, D. Bauer, S. V. Popruzhenko, and M. J. J. Vrakking, "Time-resolved holography with photoelectrons," Science **331**, 61–64 (2011).
4. D. G. Arbo, S. Yoshida, E. Persson, K. I. Dimitriou, and J. Burgdorfer, "Interference oscillations in the angular distribution of laser-ionized electrons near ionization threshold," Phys. Rev. Lett. **96**, 143003 (2006).
5. A. Rudenko, K. Zrost, C. D. Schroter, V. L. B. de Jesus, B. Feuerstein, R. Moshammer, and J. Ullrich, "Resonant structures in the low-energy electron continuum for single ionization of atoms in the tunnelling regime," J. Phys. B **37**, L407–L413 (2004).
6. L. D. Landau and E. M. Lifshitz, *Quantum Mechanics*, 3rd ed. (Butterworth-Heinemann, 1981)
7. Z. Sun, J. Chen, and W. Rudolph, "Determination of the transient electron temperature in a femtosecond-laser-induced air plasma filament," Phys. Rev. E **83**, 046408 (2011).
8. S. Tzortzakis, B. Prade, M. Franco, and A. Mysyrowicz, "Time-evolution of the plasma channel at the trail of a self-guided IR femtosecond laser pulse in air," Opt. Commun. **181**, 123–127 (2000).
9. Y. H. Chen, S. Varma, T. M. Antonsen, and H. M. Milchberg, "Direct measurement of the electron density of extended femtosecond laser pulse-induced filaments," Phys. Rev. Lett. **105**, 215005 (2010).
10. P. Agostini, F. Fabre, G. Mainfray, G. Petite, and N. K. Rahman, "Free-free transitions following 6-photon ionization of xeon atoms," Phys. Rev. Lett. **42**, 1127–1130 (1979).

11. M. Wickenhauser, X. M. Tong, D. G. Arbo, J. Burgdoerfer, and C. D. Lin, "Signatures of tunneling and multiphoton ionization in the electron-momentum distributions of atoms by intense few-cycle laser pulses," Phys. Rev. A **74**, 041402 (2006).
12. G. G. Paulus, F. Grasbon, H. Walther, P. Villoresi, M. Nisoli, S. Stagira, E. Priori, and S. De Silvestri, "Absolute-phase phenomena in photoionization with few-cycle laser pulses," Nature **414**, 182–184 (2001).
13. A. A. Silaev and N. V. Vvedenskii, "Residual-current excitation in plasmas produced by few-cycle laser pulses," PRL **102**, 115005 (2009).
14. see, e.g. H. Haug and S. W. Koch, *Quantum Theory of the Optical and Electronic Properties of Semiconductors*, 5th ed. (World Scientific Publ., 2009), Chap. 8.
15. C. Jacoboni and P. Lugli, *The Monte Carlo Method for Semiconductor Device Simulation* (Springer-Verlag, 1989).
16. see, e.g., R. Brunetti, C. Jacoboni, A. Matulionis, and V. Dienys, "Effect of interparticle collisions on energy relaxation of carriers in semiconductors," Physica B **134**, 369–373 (1985) for self-scattering method for el.-el. Coulomb scattering.

---

1. Introduction

The interaction of atoms and molecules with an intense ultrashort laser pulse (USP) plays a decisive role in a wide range of modern physics including high-harmonic generation (HHG) [1], pulse propagation, and filamentation in gases [2]. Besides the USP induced ionization process itself, an interesting question concerns the characterization of the generated electrons and ions and their coupling to electromagnetic fields.

Due to the fundamental quantum mechanical energy, momentum, and angular momentum conservation laws, the strong-field ionization initially generates highly anisotropic angular (momentum) photoionized electron/ion distributions. The precise nature of these distributions depends sensitively on the ionizing femtosecond pulse, in particular its peak intensity, duration, polarization state, wavelength, pulse shape, and the species (atom or molecule) being ionized. Quite recently it has become possible to experimentally analyze these distributions using novel electron holographic techniques based on velocity imaging measurements [3] that generate ultrafast, high resolution snapshots of the ionization process and allow for quantitative comparison with rigorous theory and simulation.

In this paper, we present a microscopic analysis of the short-time dynamics of photoionized electrons created by an intense few cycle laser pulse and initially correlated with their parent nucleus. We use Monte-Carlo methods to simulate the electron relaxation processes governed by their mutual Coulomb interaction and the scattering from ions.

Initially, the photoionized electrons occupy the states of anisotropic momentum and angular momentum distributions and take a time, longer than the current ionizing pulse, to relax toward a genuine electron plasma. Such a plasma is characterized by a Fermi-Dirac quasi-equilibrium distribution which is fully defined by the electron density and their kinetic energy, i.e. the plasma temperature. Clearly such a distribution is completely isotropic, depending on the absolute value of the carrier momentum only. Due to the basic conservation laws of Coulomb-induced carrier relaxation, the carrier density, total momentum and the kinetic carrier energy remain unchanged in the carrier kinetics. Hence, the anisotropy of the carrier distributions is the important quantity on which basis one can determine how far the electron distribution is removed from a real plasma state. Our microscopic modeling allows us to identify and quantitatively characterize the nonequilibrium regime where the anisotropy of the distributions might play an important role. Based on these results, we identify the physical conditions and the characteristic timescales after which the use of isotropic equilibrium plasma models becomes justified.

2. Theoretical approach

To investigate the ionization process and the evolution from the individual electron distribution into the state of a collective plasma, we have to solve the nonlinear light-matter interaction and the many-body dynamics governed by the electron-light, electron-electron and electron-ion Coulomb interactions. Here, the relevant equation is the quantum Boltzmann equation (BME) for a Wigner function $f_W^e(\mathbf{r}, \mathbf{k}, t)$ which is generally a function of space and momentum coordinates as well as time. The BME includes drift and diffusion terms, the interaction with external fields, collision integrals as well as ionization and recombination terms

$$\left[\frac{\partial}{\partial t} + \frac{\hbar \mathbf{k}}{m_e} \cdot \nabla_{\mathbf{r}} - \frac{1}{\hbar}(\nabla V) \cdot \nabla_{\mathbf{k}}\right] f_W^e(\mathbf{r}, \mathbf{k}, t)$$

$$= \frac{\partial}{\partial t} f_W^e(\mathbf{r}, \mathbf{k}, t)|_{collision} + \frac{\partial}{\partial t} f_W^e(\mathbf{r}, \mathbf{k}, t)|_{ionization} + \frac{\partial}{\partial t} f_W^e(\mathbf{r}, \mathbf{k}, t)|_{recombination}. \tag{1}$$

Ignoring the collision, ionization and recombination on the right hand side of the equation and inserting the Lorentz force $-\nabla V = q_e(\mathbf{E} + \mathbf{v} \times \mathbf{B})$ with $\hbar \mathbf{k} = m_e \mathbf{v}$ in the drift term leads to the Vlasov equation. Ideally, one would have to treat the full problem of strong-field ionization together with the many-body dynamics at the level of quantum kinetic theory. However, for realistic systems, the numerical solution of the complete process described by Eq. (1) is not feasible with current-day computer resources.

Fortunately, for the case of ultrashort-pulse photo-ionized electrons in dilute gases, the full problem can be simplified considering the basic physical conditions. The ionization with the high intensity light pulses happens on the timescale of several femtoseconds whereas for typical electron densities around $10^{23}/m^3$ the inverse plasma frequency is up to one picosecond. This allows for the separation of the ionization and relaxation dynamics. Furthermore, a typical length scale for electrons should be around the Bohr radius ($a_B \simeq 0.05\,nm$). In contrast typical laser wavelengths (several 100 nm) or filament diameters (around $50\,\mu m$) are much larger. Therefore, we can restrict the electron dynamics after the ionization to an evolution on the electronic length scale of a quasi-homogeneous electron gas which allows for dropping the space coordinate. Even with these approximations, the numerical solution still remains very time demanding.

To demonstrate the feasibility of this scheme, we treat a dilute gas of hydrogen atoms interacting with an intense short laser pulse. This choice allows us to avoid any electron correlation effects during the nonlinear ionization process by the field, which need to be approximated for other atomic systems. Furthermore, it is has been shown [4] that momentum distributions obtained for the hydrogen atom are in excellent agreement with experimental data for noble gas atoms [5] which demonstrates that the exact form of the atomic Coulomb potential does not influence the qualitative ionization features.

We determine the initial momentum distribution of the electrons following strong field photoionization by solving the time-dependent Schrödinger equation of an individual hydrogen atom in dipole approximation:

$$i\hbar \frac{\partial}{\partial t} \Psi(\rho, z; t) = \left[\frac{\mathbf{p}^2}{2m_e} - \frac{e^2}{4\pi\varepsilon_0 r} + eE(t)z\right] \Psi(\rho, z; t) \tag{2}$$

where $\mathbf{r} = (\rho, z, \phi)$ and $\mathbf{p}$ are the coordinate and the conjugate momentum operator of the electron. We assume an exciting linearly in z-direction polarized laser pulse represented by the electric field

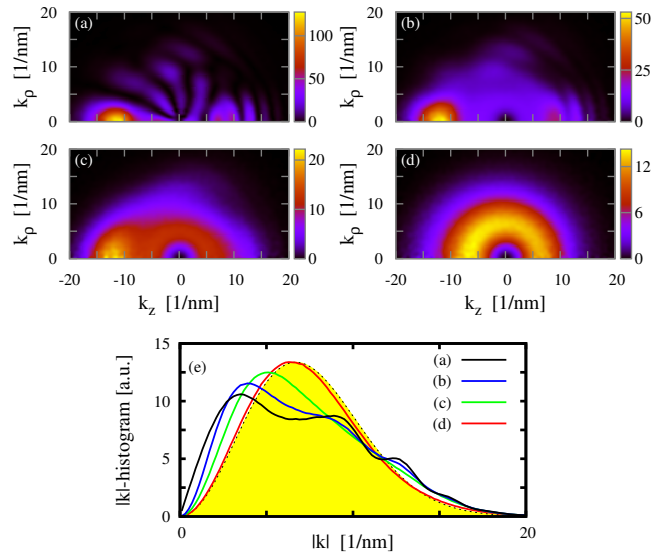$$E(t) = E_0 \sin^2\left(\frac{\pi t}{T}\right) \sin(\omega t + \chi). \tag{3}$$

Fig. 1. Relaxation of an anisotropic nonequilibrium electron distribution created by ionizing hydrogen atoms with a $400\,nm$ 3-cycle pulse of intensity $I = 1 \times 10^{14} W/cm^2$. Above, $H(k,\theta)$ for different times in units of $1/f_{pl}(N^e)$ (a) $t = 0$, (b) $t = 0.31$, (c) $t = 1.04$ and (d) $t = 6.25$. Here, $k_z = k\cos(\theta)$ and $k_\rho = k\sin(\theta) = (k_x^2 + k_y^2)^{1/2}$. Below, in (e) the corresponding θ-angle integrated $\bar{H}(k)$. The yellow area shows the final Fermi Dirac distribution with $T = 19797\,K$ and $\bar{E} = 2.559\,eV$ for (e). The total electron density is $N^e = 2.155 \times 10^{23}/m^3$ which corresponds to an inverse 3D plasma frequency $1/f_{pl}(N^e) = 0.240\,ps$.

with E_0, $\hbar\omega$, χ and T are the peak amplitude, frequency, carrier-to-envelope phase and total duration of the pulse. Since the Hamiltonian in the time-dependent Schrödinger equation (2) is symmetric with respect to rotations over the polarization axis z, the solution $\Psi(\rho,z;t)$ does not depend on the angle ϕ. We discretize the Schrödinger equation on a spatial grid with spacings $\Delta\rho = \Delta z = 0.1$ a.u. and use a time step of $\Delta t = 0.03$ a.u. Grid sizes of up to 1200 and 8000 points in ρ and z directions, respectively, are implemented with $\cos^{1/6}$ mask functions at the edges. The grids were large enough to keep the configuration space wavefunction on the grid for analysis of the momentum distributions. We have checked that the results are not influenced by the boundary conditions. The solution $\Psi(\rho,z;t)$ is propagated using the Crank-Nicolson method and the wave function of the (initial) $1s$ ground state of the hydrogen atom is obtained by imaginary time propagation. The electron momentum distributions are obtained by projection of the full configuration space wavefunction at the end of the pulse onto the analytical solutions of the outgoing continuum wave function, as given in the literature (e.g. [6]), represented on the grid.

Examples of the computed photoelectron momentum distributions are shown in Figs. 1 (a), 2 (a) and 3 (a) for $400\,nm$ pulses with 3 or 6 cycles, respectively. The assumed densities are in the range of the values reported in the literature, i.e. a few $10^{23}/m^3$ [7,8] or around $5 \times 10^{22}/m^3$ [9]. These distributions are rotationally symmetric around the polarization direction of the light field, the z-axis. We clearly see that the initial distributions are highly anisotropic, which is in agreement with results of previous calculations obtained in a similar parameter regime [4].

In each case a minimum number of 5 photons needs to be absorbed from the field to photoionize the hydrogen atom. However, absorption of more photons is likely and leads to the generation of electrons with larger momenta. The different orders of this above threshold ion-
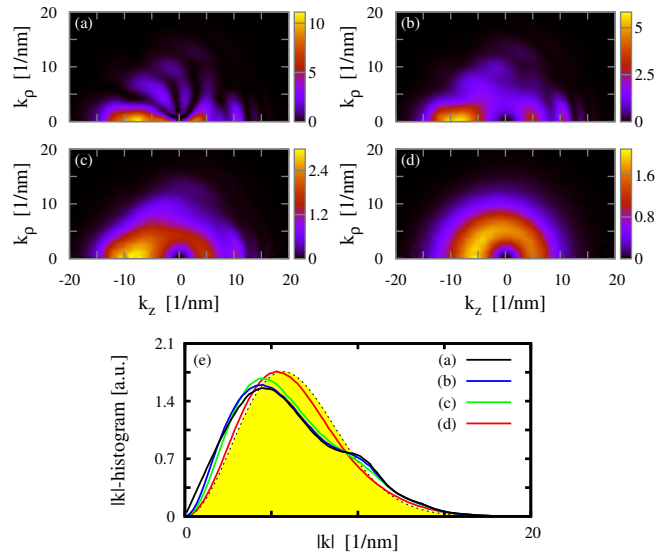
Fig. 2. Relaxation of an anisotropic nonequilibrium electron distribution created by ionizing hydrogen atoms with a $400\,nm$ 3-cycle pulse of intensity $I = 5 \times 10^{13} W/cm^2$. Above, $H(k,\theta)$ for different times in units of $1/f_{pl}(N^e)$ (a) $t = 0$, (b) $t = 0.31$, (c) $t = 1.04$, (d) $t = 6.27$. Below, in (e) the corresponding θ-angle integrated $\bar{H}(k)$. The yellow area shows the final Fermi Dirac distribution with $T = 14273\,K$ and $\bar{E} = 1.845\,eV$. The total electron density in (a)-(e) is $N^e = 2.402 \times 10^{22}/m^3$ which corresponds to an inverse 3D plasma frequency $1/f_{pl}(N^e) = 0.718\,ps$.

ization process (ATI, [10]) are clearly seen for the longer pulse as a series of concentric rings separated by $\Delta k = \sqrt{2m_e\hbar\omega}$, where m_e is the mass of the electron [11]. The ATI rings do not appear in the case of the 3-cycle pulse, since the ATI process can be understood as interference between electron wavepackets generated at two successive field maxima of (nearly) the same amplitude, which is not fulfilled for an ultrashort 3-cycle pulse. Thus, in these cases for the relatively low intensities $I = 1 \times 10^{14} W/cm^2$ (Fig. 1) and for $I = 5 \times 10^{13} W/cm^2$ (Fig. 2) the initial distributions in k (black lines in panels (e)) are broad without significant structure in form of maxima and minima. However, the average energy absorbed from the field mainly depends on the wavelength and the intensity of the laser pulse. Therefore, it is approximately the same in Figs. 2(a) and 3(a) (both obtained for an intensity of 5×10^{13} w/cm²) but it is different in Fig. 1(a) (obtained at 1×10^{14} W/cm²). Please also note, that in the 3-cycle case the distributions show a strong asymmetry with respect to $k_z = 0$. This indicates that the ionization process strongly depends on the carrier-to-envelope phase, which is chosen as $\chi = \pi/2$ in the present calculations. In agreement with experimental observations [12] the asymmetry almost disappears for the 6-cycle pulse. This anisotropy leads to a non-vanishing average momentum $\bar{k}_z$ of the photoionized electrons, i.e. a dc current $J_z \propto \bar{k}_z$. However, this current will be damped, e.g., by the many-body Coulomb scattering. Values of the average momentum $\bar{k}_z$ for different times after the ionization are shown in section 3. A detailed investigation of the current strength depending on the pulse parameters can be found in [13].

For the relaxation dynamics of the anisotropic electron momentum distributions and the process of quasi-equilibrium plasma formation, we solve the quantum Boltzmann equation (1) with the previously introduced approximations. Since the electron-ion recombination happens on a nanosecond [7] timescale, the number of free electrons and ions is approximately conserved
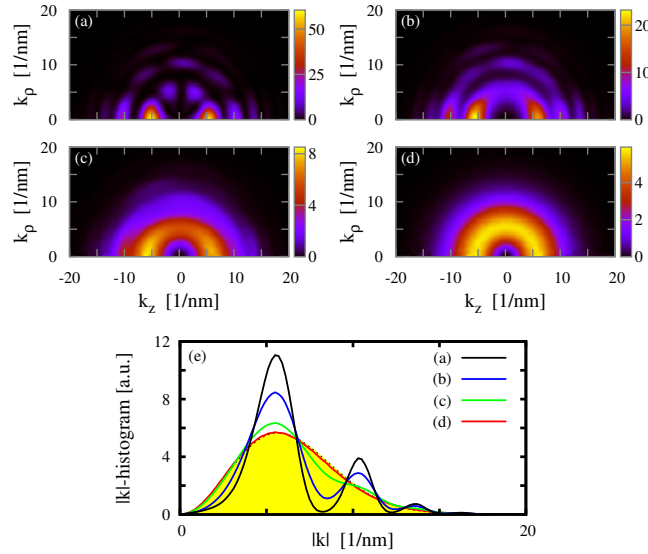
Fig. 3. Relaxation of an anisotropic nonequilibrium electron distribution created by ioniz-ing hydrogen atoms with a $400\,nm$ 6-cycle pulse of intensity $I = 5 \times 10^{13} W/cm^2$. Above, $H(k,\theta)$ for different times (a) $t = 0/f_{pl}$, (b) $t = 0.25/f_{pl}$, (c) $t = 1/f_{pl}$, (d) $t = 5/f_{pl}$. Below, in (e) $\bar{H}(k)$ for the same times. The yellow area shows the final Fermi Dirac dis-tribution ($T = 14283\,K$, $\bar{E} = 1.846\,eV$). The total electron density is $N^e = 7.743 \times 10^{22}/m^3$ corresponding to an inverse 3D plasma frequency of approximately $1/f_{pl}(N^e) = 0.400\,ps$.

during the carrier relaxation into the quasi-equilibrium collective plasma state. Thus in the ab-sence of further external fields – as the already gone ionizing pulse –, the BME reduces to its collision integrals,

$$\partial_t f_k^e|_{e-\lambda\,\text{collision}} = \frac{2\pi}{\hbar}\sum_{\mathbf{p},\mathbf{q}} V_{|\mathbf{q}|}^2 (1-f_{\mathbf{k}}^e)(1-f_{\mathbf{p}}^\lambda)f_{\mathbf{k}-\mathbf{q}}^e f_{\mathbf{p}+\mathbf{q}}^\lambda \delta(\Delta E_{\mathbf{k},\mathbf{p},\mathbf{q}}^{e,\lambda})$$

$$- \frac{2\pi}{\hbar}\sum_{\mathbf{p},\mathbf{q}} V_{|\mathbf{q}|}^2 f_{\mathbf{k}}^e f_{\mathbf{p}}^\lambda (1-f_{\mathbf{k}-\mathbf{q}}^e)(1-f_{\mathbf{p}+\mathbf{q}}^\lambda) \delta(\Delta E_{\mathbf{k},\mathbf{p},\mathbf{q}}^{e,\lambda})$$

$$\lambda \in \{e,i\}, \Delta E_{\mathbf{k},\mathbf{p},\mathbf{q}}^{e,\lambda} = \frac{\hbar^2|\mathbf{k}|^2 - \hbar^2|\mathbf{k}-\mathbf{q}|^2}{2m_e} + \frac{\hbar^2|\mathbf{p}|^2 - \hbar^2|\mathbf{p}+\mathbf{q}|^2}{2m_\lambda} \qquad (4)$$

where $f_{\mathbf{k}}^\lambda$ and m_λ denote the momentum dependent probability distribution and mass of the electrons ($\lambda = e$) and ions ($\lambda = i$), respectively. The δ-distribution $\delta(E)$ provides the energy conservation during the scattering.

The Coulomb potential $V_{\mathbf{q}}$ is screened using a Debye screening constant κ_D which is obtained as the $q = 0$-limit of the static Lindhard formula [14] for the final equilibrium distributions. Due to their large mass the ions hardly contribute to the screening.

Many properties of the Boltzmann Coulomb collision integral are well known. The long-term equilibrium solution is a Fermi-Dirac distribution which approaches a Boltzmann distribution in the non-degenerate limit. Furthermore, the Coulomb collisions conserve the particle num-ber, the total momentum and total energy of the electron-ion gas but allow for the exchange of momentum and energy between the individual particles. Due to the large mass difference of electrons and ions the electron ion scattering is pretty much restricted to elastic scattering events where the absolute values of the electron momentum $|\mathbf{k}| \simeq |\mathbf{k} - \mathbf{q}|$ and the ion momen-

tum $|\mathbf{p}| \simeq |\mathbf{p}+\mathbf{q}|$ are conserved. As a consequence, the electron-ion interaction is only relevant for anisotropic initial conditions where the electron-ion interaction contributes to the reduction of the anisotropy and is the only way to change the average momentum of the electron system. Furthermore, in the non-degenerate limit only the total number of ions contributes to the electron dynamics which effectively decouples the ion and electron dynamics.

Under these conditions, the final equilibrium distribution of the electrons is determined once we know the number of free electrons generated and their average energy $\bar{E}$. Even for typical experimental conditions of strong short-pulse ionization – as considered here – we are still in the non-degenerate limit such that $(1 - f_{\mathbf{k}}^{\lambda}) \simeq 1$. This allows for direct determination of the temperature T of the final equilibrium electron plasma by the well-known property $\bar{E} = 3/2k_B T$ of Boltzmann distributions.

To describe the dynamic evolution of the probability distribution, we numerically solve the Boltzmann collision integral. Due to the high dimensionality of the momentum integrals, a direct integration using e.g. a Runge-Kutta method is unpractical. Therefore, we resort to the Monte-Carlo technique which is widely used for these kind of problems, e.g. in semiconductor device simulations [15]. To efficiently evaluate the electron-electron scattering rates in our anisotropic configuration, we use the so-called self-scattering method introduced by Brunetti et al. [16]. Due to the highly anisotropic initial distribution, we have to simulate up to 10^7 particles.

For a quantitative analysis of the relaxation dynamics, we calculate the distribution functions $f(k,\theta)$ in spherical coordinates using the momentum-histograms of the simulated particles. Taking advantage of the ϕ symmetry we have already dropped any ϕ-angle dependence here and introduce for use in Fig. 1–4

$$H(k,\theta) = \frac{k^2}{4\pi^2} f(k,\theta) \tag{5}$$

and for comparison its θ-angle integrated version

$$\bar{H}(k) = \frac{1}{2} \int_0^\pi sin(\theta) H(k,\theta) \, d\theta. \tag{6}$$

In case of isotropy $H(k,\theta)$ will match $\bar{H}(k)$. Taking snapshots of these functions will allow us to follow the isotropization of the initially anisotropic distribution and determine an estimate of the time after which an isotropic plasma like answer of the electrons can be expected.

3. Results and discussion

We start from the initial distributions of Figs. 1-3 (a) and compute the dynamical evolution until quasi-equilibrium is reached. Characteristic snapshots of the obtained distributions $H(k,\theta)$ are shown in parts (b), (c), and (d) of Figs. 1-3. Here, part (c) is taken at the inverse plasma frequency – a characteristic timescale for a plasma – and (d) corresponds to a time where the final isotropic equilibrium state is nearly reached. The time development of $\bar{H}(k)$ is plotted in parts (e). We notice that the quasi-discrete MPI structures are smeared out within the first $100\,fs$. The entire distributions relax on the order of picoseconds to nearly isotropic equilibrium distributions which have temperatures of $14000\,K$ for the lower intensity case Figs. 2 and 3 as well as $20000\,K$ for the higher one in Fig. 1, respectively.

For a more quantitative analysis of the relaxation dynamics and in order to extract the characteristic relaxation times, we define the function

$$r(t) = \frac{\int dk\,sin(\theta)d\theta\,|H(k,\theta,t) - H(k,\theta,equilibrium)|}{\int dk\,sin(\theta)d\theta\,|H(k,\theta,t=0) - H(k,\theta,equilibrium)|} \tag{7}$$
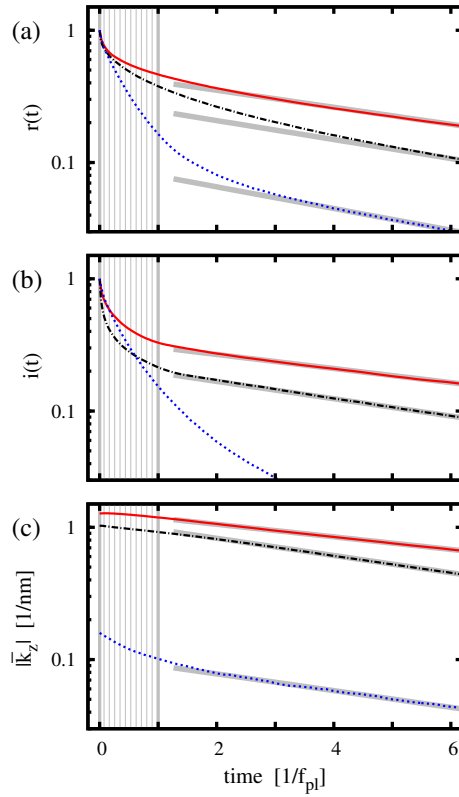
Fig. 4. Relaxation times calculated from $H(k,\theta)$ (a), the calculated anisotropy (b) and the average k_z momentum (c) for the ionization conditions: $400\,nm$ pulse with 3 cycles and $I = 5 \times 10^{13} W/cm^2$ (solid, red) as well as $I = 1 \times 10^{14} W/cm^2$ (dashed dotted, black) and a $400\,nm$ pulse 6 cycles pulse of intensity $5 \times 10^{13} W/cm^2$ (dotted, blue). The time is given in units of $1/f_{pl}$, i.e. $0.718\,ps$ (red), $0.240\,ps$ (black) and $0.400\,ps$ (blue). The short-time relaxation dynamics happens in the regime below $1/f_{pl}$. The gray lines are exponential fits to the long-time dynamics.

which shows the deviation of the time dependent distribution from the corresponding final Fermi-Dirac distribution. Furthermore, we introduce

$$i(t) = \frac{\int dk\,sin(\theta)d\theta\,|H(k,\theta,t) - \bar{H}(k,t)|}{\int dk\,sin(\theta)d\theta\,|H(k,\theta,t=0) - \bar{H}(k,t=0)|} \qquad (8)$$

which as the difference of the time dependent distribution and the corresponding angle averaged isotropic distribution allows for the measurement of the anisotropy of the photoionized electrons. Within a time interval where the real dynamics can be approximated by a relaxation time approach both functions will show a line in a log plot with slope $1/\tau$.

Figure 4 shows (a) the relaxation time $r(t)$, (b) the anisotropy i(t) and (c) the average k_z momentum for the initial conditions of Fig. 1-3. In all cases, we show the time in units of the inverse plasma frequency $1/f_{pl} = 2\pi[N^e q_e^2/(m_e \varepsilon_0)]^{-1/2}$. Assuming that $1/f_{pl}$ defines the characteristic timescale this scaling transforms the relaxation dynamics to a similar time frame. Analyzing the results, we note that the relaxation dynamics can be divided into two part. At the beginning the significant features of the ionization probability are smeared out and the

major part of the anisotropy is removed (striped areas in Fig. 4). In other words, the short term dynamics is dominated by the loss of anisotropy which obviously cannot be approximated by a simple relaxation time model (cp. Fig. 4a). This anisotropy indicates that the electrons are not yet in a plasma state which should be measurable, e.g., in THz experiments. The relaxation to a totally isotropic static equilibrium distribution happens on the much longer time-sale of a few picoseconds. In case of the ionization with the 3-cycle pulse, the dominating part of this long time dynamics is the decrease of the average k_z momentum. This process – governed by the electron-ion scattering – shows a similar linear dependence in the log plots of Fig. 4, i.e., in (a) $\tau = 6.76/f_{pl}$ (red), $\tau = 6.06/f_{pl}$ (black) and $\tau = 5.3/f_{pl}$ (blue), (b) $\tau = 8.17/f_{pl}$ (red), $\tau = 6.63/f_{pl}$ (black), or in (c) $\tau = 9.15/f_{pl}$ (red), $\tau = 6.76/f_{pl}$ (black) and $\tau = 6.87/f_{pl}$ (blue). A value for the blue line in (b) cannot be extracted. Generally, we see that the inverse plasma frequency indeed yields a rough estimate for the scaling of the time evolution.

4. Conclusion

In summary, our investigations clearly show that the high-intensity short-pulse ionization of atoms leads to highly anisotropic electron distributions. Our quantum Boltzmann analysis allows us to identify two characteristic dynamical regimes during which the initial nonequilibrium distribution approaches a quasi-equilibrum plasma state. Due to the elastic and inelastic Coulomb scattering the electrons relax in a first step towards a hot nonequilibrium isotropic distribution. This is followed in a second step by a slower relaxation towards a Boltzmann distribution which is then indicative of a quasi-equilibrium, fully isotropic plasma state. An open remaining question is how general electromagnetic fields (optical, THz, etc.) couple to these nonequilibrium, initially anisotropic photoionized electron distributions.